

Supplemental Information for

Understanding structural incorporation of oxygen vacancies in perovskite cobaltite films and potential consequences for electrocatalysis

Lei Jin,^{a†*} Feng Zhang,^{b†} Felix Gunkel,^c Xian-Kui Wei,^a Yanxing Zhang,^d Dawei Wang,^{b*} Juri Barthel,^{a,e} Rafal E. Dunin-Borkowski,^{a,f} and Chun-Lin Jia^{a,b}

a Ernst Ruska-Centre for Microscopy and Spectroscopy with Electrons (ER-C), Forschungszentrum Jülich GmbH, 52425 Jülich, Germany.

b School of Microelectronics and State Key Laboratory for Mechanical Behavior of Materials, Xi'an Jiaotong University, Xi'an 710049, China.

c Peter Grünberg Institute (PGI-7), Forschungszentrum Jülich GmbH, 52425 Jülich, Germany

d School of Physics, Henan Normal University, Xinxiang 453007, China

e Central Facility for Electron Microscopy, RWTH Aachen University, 52074 Aachen, Germany

f Peter Grünberg Institute (PGI-5), Forschungszentrum Jülich GmbH, 52425 Jülich, Germany

† Equal contribution.

* Corresponding authors. E-mail: l.jin@fz-juelich.de (L.J.) and dawei.wang@xjtu.edu.cn (D.W.)

Supplemental Table 1. Parameters used for the simulated images under negative spherical aberration imaging (NCSI) conditions, which show the best fit to the experimental images of high (Figure 4; HCM), medium (Supplemental Figure S5; MCM), and low (Supplemental Figure S6; LCM) contrast modulation areas. The semi-convergent angle and the focus spread were set to 0.3 mrad and 3 nm for all simulations, respectively.

Parameters	HCM area	MCM area Magnitude	LCM area
Specimen thickness	4.4 nm	4.4 nm	4.8 nm
Specimen tilt	(0.0, 1.9) mrad	(-0.3, 2.1) mrad	(1.2, -2.3) mrad
Absorption	0.018	0.018	0.018
Image spread	20 pm	20 pm	26 pm
Overfocus C_1	3.56 nm	3.76 nm	2.85 nm
Two-fold astigmatism A_1	(0.1, 0.4) nm	(-1.2, 0.1) nm	(0.0, -0.3) nm
Three-fold astigmatism A_2	(-35, -34) nm	(93, 27) nm	(17, 12) nm
Coma B_2	(-18, -16) nm	(-24, -68) nm	(-19, -95) nm
3 rd -order spherical aberration C_3	-13 μ m	-13 μ m	-14 μ m
5 th -order spherical aberration C_5	4 mm	4 mm	4 mm
$B_{Pr,Ba}$		0.0053 nm ²	
B_{Co}		0.0021 nm ²	
$B_{O(1)}$		0.0052 nm ²	
$B_{O(2)}$		0.0055 nm ²	

Note: Parameters of specimen tilt, A_1 , A_2 and B_2 are given in the format of (horizontal component, vertical component). Isotropic B parameters for Debye-Waller factors were taken from ICSD 164818 for room temperature PrCoO₃, as no existing data for Pr_{0.5}Ba_{0.5}CoO₃ was found in literature.

Supplemental Note 1:

We note, in Figure 4a the oxygen columns exhibit an elongated shape, which are still not perfectly reproduced by the simulation as shown in Figure 4b. We consider the possible reasons as follows:

- i) In the raw image Figure 3a, individual oxygen columns at the same Co-O plane show position variations in the [001] direction (elongation direction), inevitably resulting in the apparent (vertical) elongation of oxygen columns in the averaged image Figure 4a;
- ii) The incorporation of oxygen vacancies may induce oxygen octahedral distortion, as suggested by our density functional theory (DFT) calculations (not shown), leading to slight relative shifts of individual oxygen atoms in an atomic column. Such a distortion, *i.e.*, oxygen atoms do not line up along the viewing direction, was not included in our simplified model used in Figure 4c.

Supplemental Figures

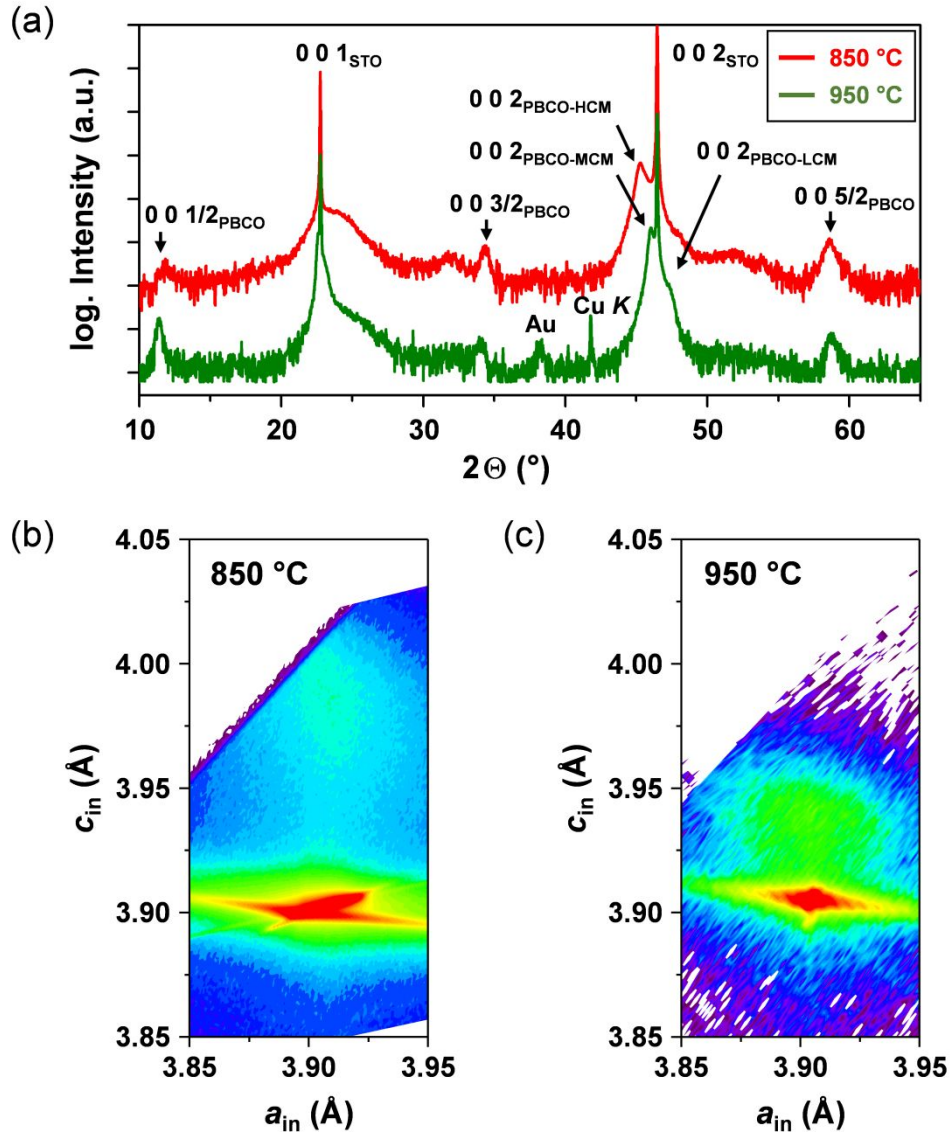


Figure S1 (a) X-ray diffraction (XRD) results showing the phase structure of the PBCO films. Superstructural diffraction peaks are labeled by $(0\ 0\ l/2)_{\text{PBCO}}$ ($l = \text{odd}$). The peaks located at the lower- and higher-angle shoulders in the vicinity of the substrate peak originate from the medium contrast modulation (MCM) and low contrast modulation (LCM) areas of PBCO grown at 950 $^{\circ}\text{C}$ (see Figure 1b in the main text), respectively, revealing the structural inhomogeneity. The peaks labeled by Au and Cu K

originate from the gold layer (deposited for focused ion beam preparation) and the X-ray source. (b) and (c) Reciprocal space map information around the SrTiO₃ (013) reflection showing the presence of in-plane lattice strain for both films.

The following issues must be emphasized:

- i) Owing to the kinematic scattering nature of XRD, the intensity of the superstructural peaks is actually dominated by the contribution of lattice/distance modulation of Pr/Ba-Pr/Ba atoms, although the modulation itself is associated with oxygen vacancy ordering. This leads to intrinsic difficulties in verifying phase structures using XRD refinement in the present case.
- ii) The intensity of superstructural peaks are also influenced by the presence of Ruddlesden-Popper (R-P) ordering, particularly for the sample grown at 850 °C.
- ii) The presence of superstructural peaks in XRD is *not* a unique criterion in distinguishing Pr/Ba cation ordered double perovskites from oxygen vacancy ordered single perovskites.

Supplemental Table 2. Out-of-plane structural parameter c derived from XRD, high-resolution scanning transmission electron microscopy (STEM) and NCSI, respectively. It should be noted that XRD represents the averaged information, while transmission electron microscopy (TEM) shows localized structure. It can be seen that within the measurement error (< 8 pm for both STEM and NCSI), the results are consistent with each other.

	XRD	STEM	NCSI
PBCO-HCM	<p>$002_{\text{PBCO-HCM}}$: Sharp peak at $\sim 45.3^\circ$ $\rightarrow c \approx 4.001 \text{ \AA}$ Supplemental Figure S1</p>	<p>$c = 3.967 \text{ \AA}$ Figure 2a,b</p>	<p>$c_{\text{low}} + c_{\text{high}} = 7.963 \text{ \AA}$ $\rightarrow c = 3.982 \text{ \AA}$ Figure 4</p>
PBCO-MCM	<p>$002_{\text{PBCO-MCM}}$: Sharp peak at $\sim 46^\circ$ $\rightarrow c \approx 3.943 \text{ \AA}$ Supplemental Figure S1</p>	<p>$c = 3.965 \text{ \AA}$ Figure 2c,d</p>	<p>$c_{\text{low}} + c_{\text{high}} = 7.983 \text{ \AA}$ $\rightarrow c = 3.992 \text{ \AA}$ Supplemental Figure S5</p>
PBCO-LCM	<p>$002_{\text{PBCO-LCM}}$: Broad shoulder at $\sim 47.5^\circ$ $\rightarrow c \approx 3.826 \text{ \AA}$ Supplemental Figure S1</p>		<p>$c_{\text{low}} + c_{\text{high}} = 7.750 \text{ \AA}$ $\rightarrow c = 3.875 \text{ \AA}$ Supplemental Figure S6</p>

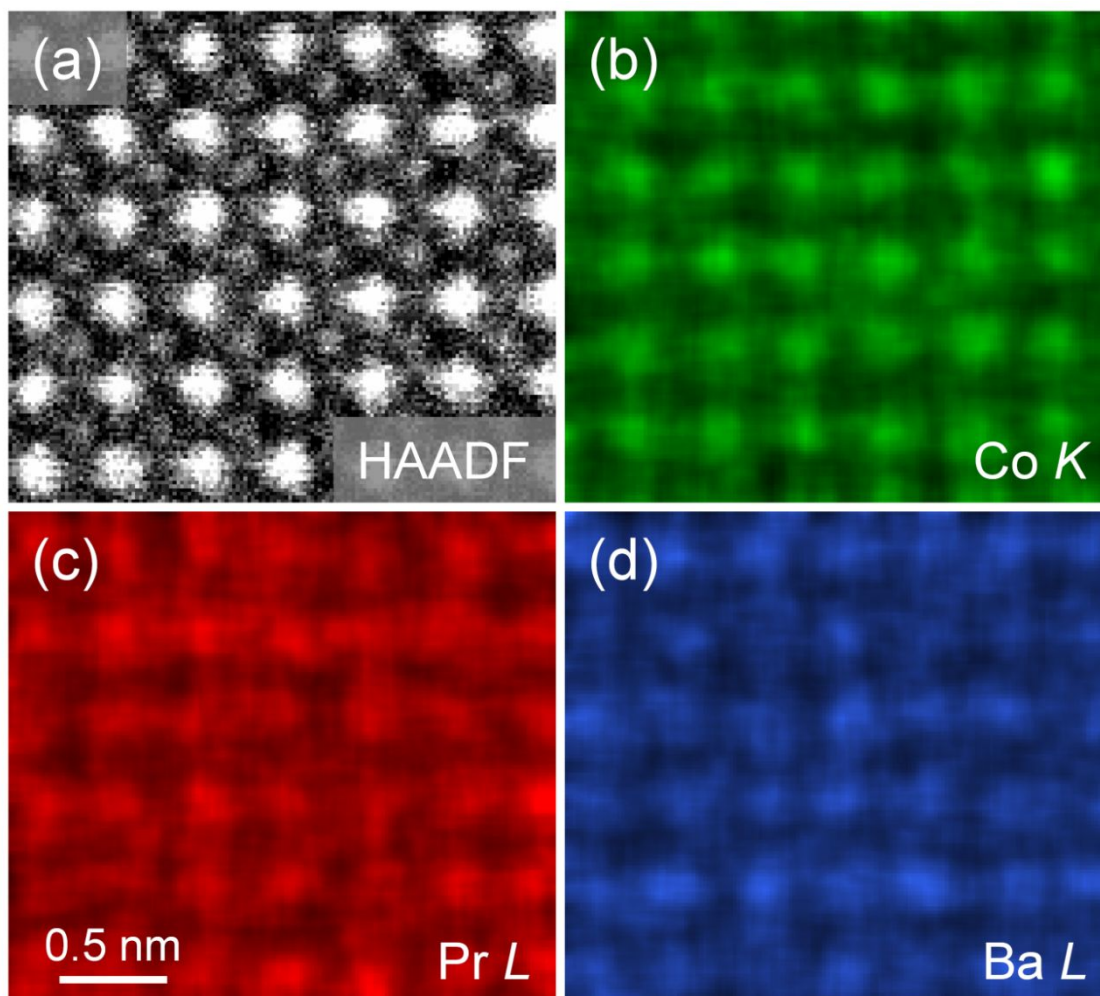


Figure S2 Atomic-resolution high-angle annular dark-field image and corresponding energy dispersive x-ray spectroscopic (EDXS) maps of Co *K*, Pr *L* and Ba *L* lines, respectively, providing evidence for the absence of A-site atomic ordering. The measured cationic ratio is $\text{Pr}_{0.51}\text{Ba}_{0.49}\text{Co}_{0.95}$. We note the error of EDXS measurement is typically on the order of 5% to 10%, for this we conclude that there is no significant deviation from the nominal value. Further measurements from different local areas show similar values for both 850 and 950 °C grown samples, suggesting that the influence of cation nonstoichiometry on the lattice expansion is minor.

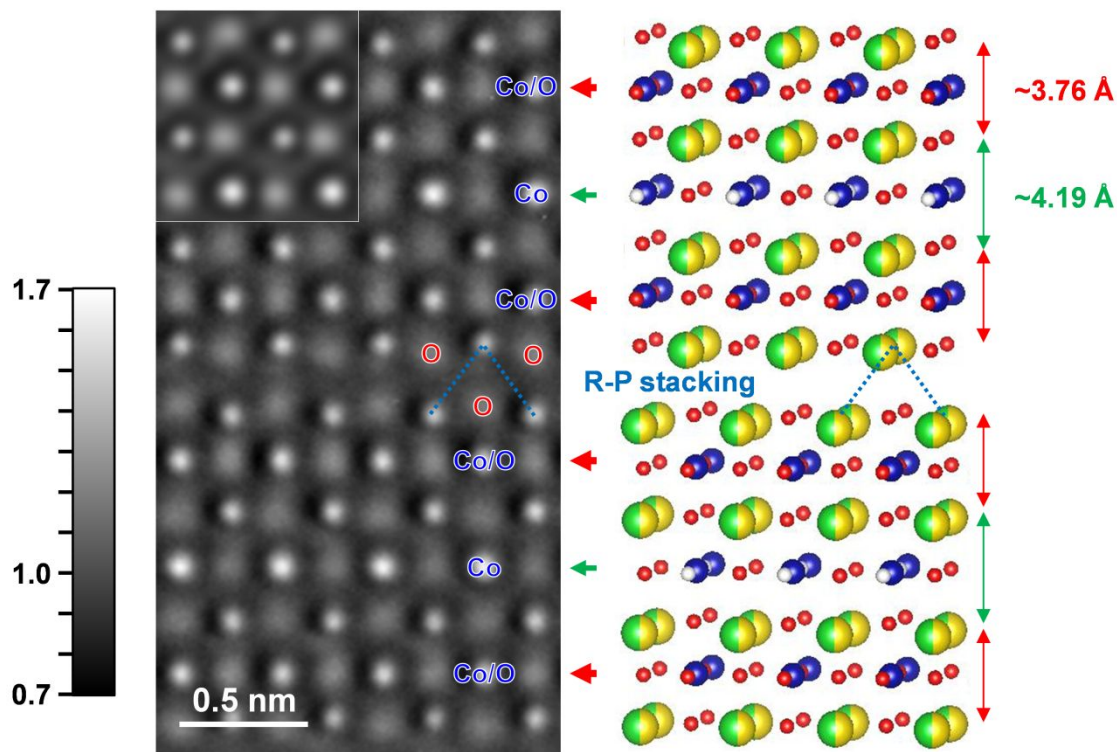


Figure S3 (Left) Negative spherical aberration image taken from the [100] direction of the sample grown at 850 °C. Inset is the best-fit simulated image. (Right) Atomic model used for the image simulation. Pr/Ba: yellow/green; Co: blue; O: red; O_{vacancy} : white. The O_{high} and O_{low} planes are marked by red and green arrows, respectively. In this viewing direction, the oxygen vacancies are ordered in the columns including Co atoms (indicated by Co) in the O_{low} planes, which leads to enhanced column intensities as compared to those columns with fully-occupied O and Co atoms (indicated by Co/O). A local Ruddlesden-Popper (R-P) stacking fault is revealed, mediated by the relative half-perovskite-unit-cell shift between the top and bottom variants.

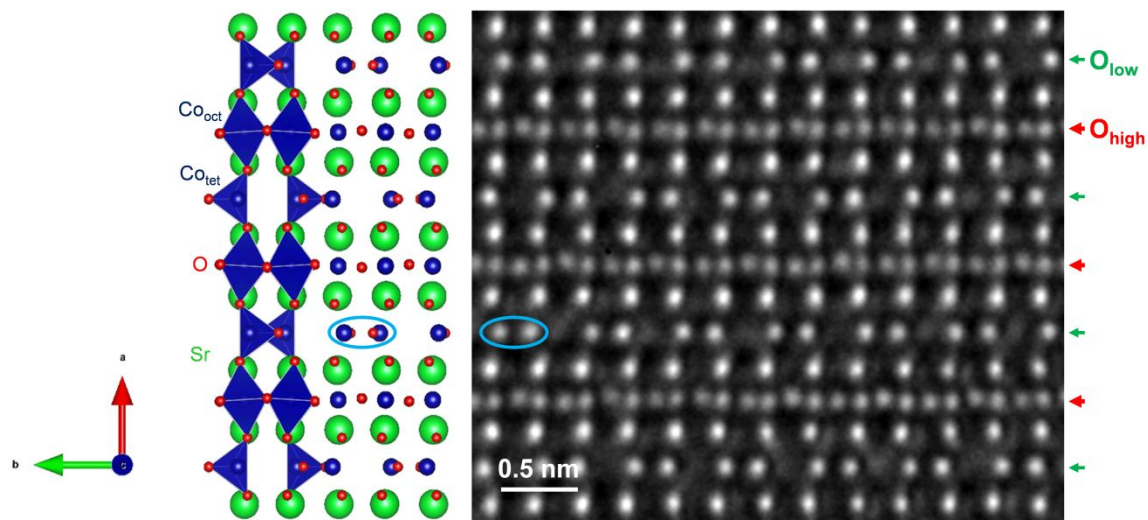


Figure S4 (Left) Atomic model of $\text{SrCoO}_{2.5}$ (ICSD 162241), a typical brownmillerite structure, projected along the pseudocubic perovskite $[110]$ direction, showing the structural response to the presence of ordered oxygen vacancies ($\delta = 0.5$). At the oxygen deficient Co-O plane (*i.e.*, O_{low}), the Co atoms are in an oxygen tetrahedral coordination environment (denote Co_{tet}), forming a pair structure marked by blue ellipses in comparison with those located in oxygen octahedra (denote Co_{oct}). (Right) Atomic-resolution image of $\text{SrCoO}_{2.5}$ recorded under NCSI conditions, showing the structural changes at Co_{tet} columns. This is clearly different from that shown in Figure 3 in the main text.

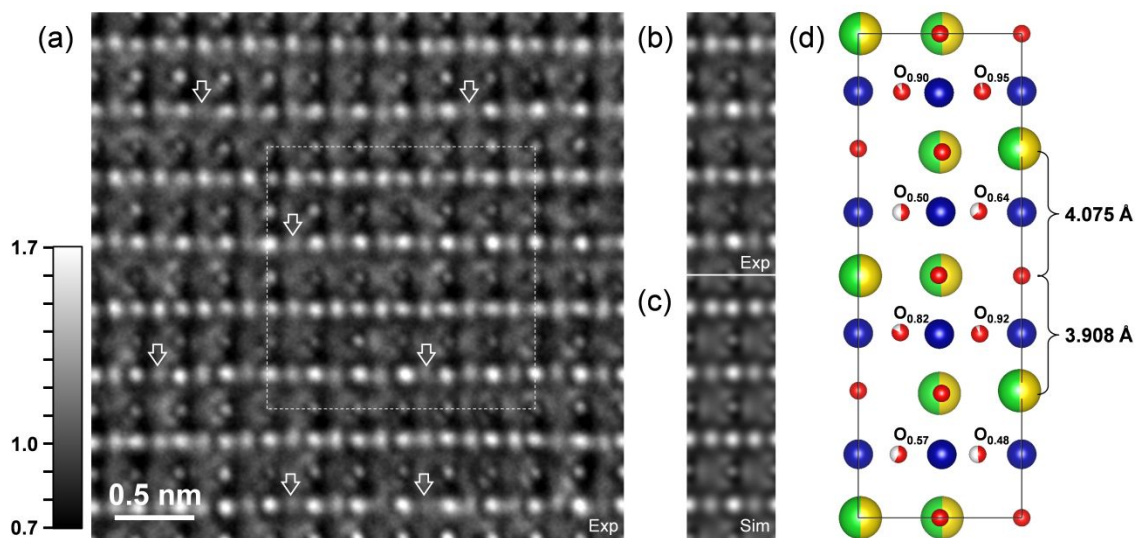


Figure S5 (a) Atomic-resolution TEM image recorded under NCSI conditions along the pseudocubic [110] direction, showing the intensity variations of O columns (*e.g.*, see columns marked by open arrows) in a medium contrast modulation region (see Figure 1b in the main text) of the 950 °C grown sample. (b) Experimental image averaged over the marked area in (a). (c) The best-fit simulated image using the atomic model shown in (d). The parameters for image simulation are listed in the Supplemental Table S1. The stacking sequence along the pseudocubic [001] can be described as ...-Pr_{0.5}Ba_{0.5}O-CoO_{2×0.55}-Pr_{0.5}Ba_{0.5}O-CoO_{2×0.9}-... (*i.e.*, Pr_{0.5}Ba_{0.5}CoO_{2.45}) and lattice distance of $c_{\text{high}} + c_{\text{low}} = 4.075 + 3.908 = 7.983 \text{ \AA}$.

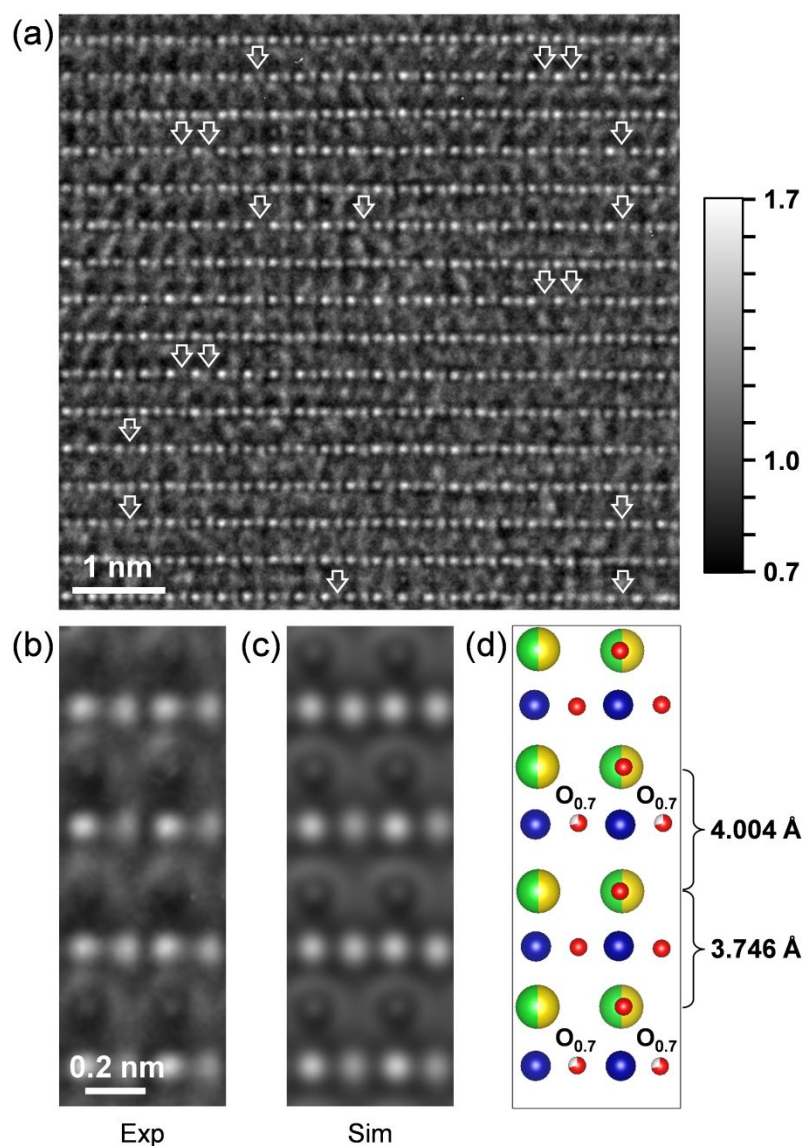


Figure S6 (a) Atomic-resolution TEM image recorded under NCSI conditions along the pseudocubic [110] direction, showing the intensity variations of O columns (*e.g.*, see columns marked by open arrows) in a low contrast modulation region (see Figure 1b in the main text) of the 950 °C grown sample. (b) Averaged experimental image and (c) the best-fit simulated image using the atomic model shown in (d). The parameters for image simulation are listed in the Supplemental Table S1. The stacking sequence along the pseudocubic [001] can be described as ...-Pr_{0.5}Ba_{0.5}O-CoO_{2×0.7}-Pr_{0.5}Ba_{0.5}O-CoO₂-... (*i.e.*, Pr_{0.5}Ba_{0.5}CoO_{2.7}) and lattice distance of $c_{\text{high}} + c_{\text{low}} = 4.004 + 3.746 = 7.750 \text{ \AA}$.

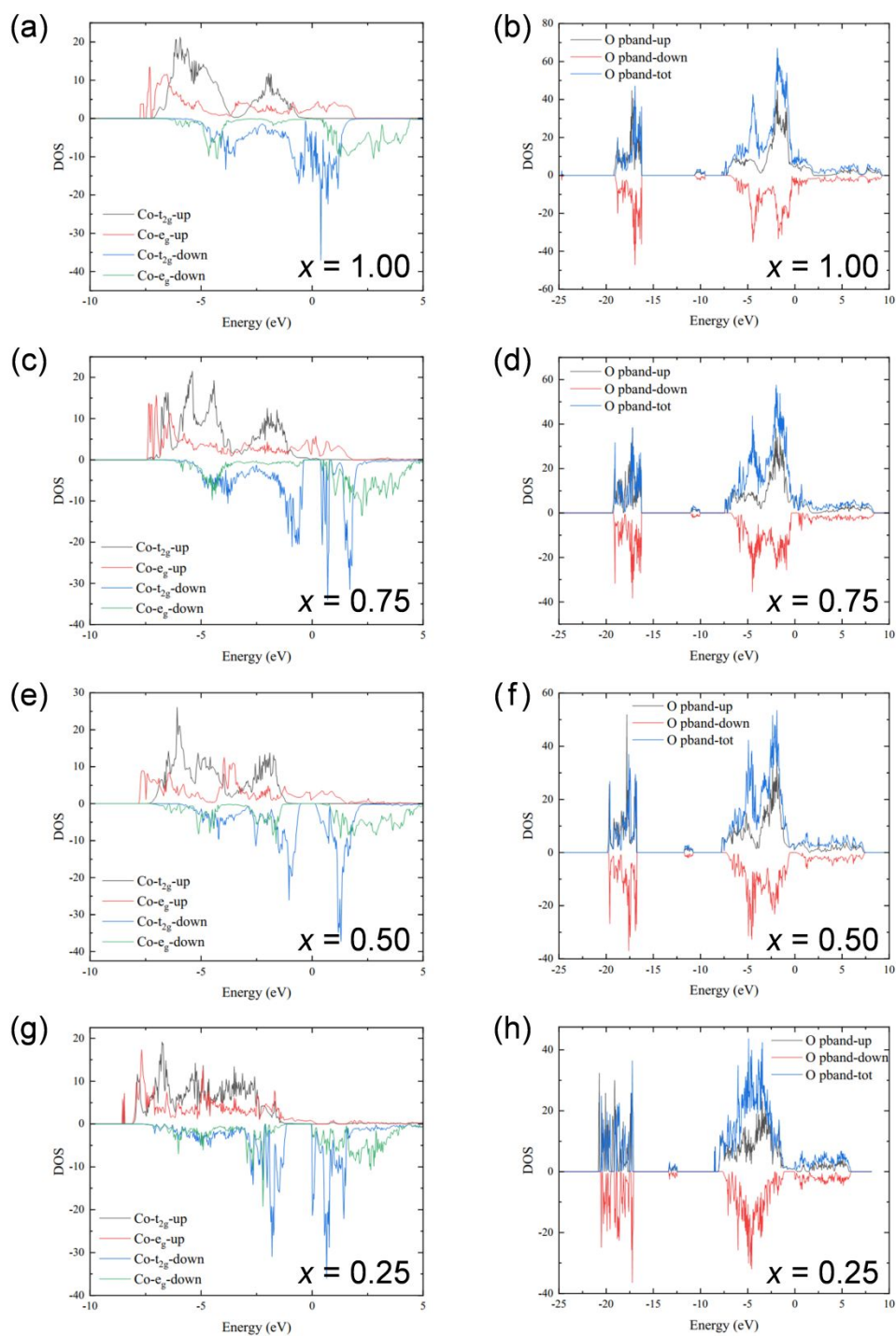


Figure S7 Density-of-states (DOS) of Co 3d orbitals and O p -bands calculated from first-principles density functional theory for different O occupancies at CoO_{2x} planes. (a,b) $x = 1.00$, (c,d) $x = 0.75$, (e,f) $x = 0.50$ and (g,h) $x = 0.25$.